



HAL
open science

Which black hole is spinning? Probing the origin of black-hole spin with gravitational waves

Christian Adamcewicz, Shanika Galaudage, Paul D Lasky, Eric Thrane

► **To cite this version:**

Christian Adamcewicz, Shanika Galaudage, Paul D Lasky, Eric Thrane. Which black hole is spinning? Probing the origin of black-hole spin with gravitational waves. *Astrophys.J.Lett.*, 2024, 964 (1), pp.L6. 10.3847/2041-8213/ad2df2 . hal-04324109

HAL Id: hal-04324109

<https://hal.science/hal-04324109v1>

Submitted on 16 May 2024

HAL is a multi-disciplinary open access archive for the deposit and dissemination of scientific research documents, whether they are published or not. The documents may come from teaching and research institutions in France or abroad, or from public or private research centers.





L'archive ouverte pluridisciplinaire **HAL**, est destinée au dépôt et à la diffusion de documents scientifiques de niveau recherche, publiés ou non, émanant des établissements d'enseignement et de recherche français ou étrangers, des laboratoires publics ou privés.



Distributed under a Creative Commons Attribution 4.0 International License



Which Black Hole Is Spinning? Probing the Origin of Black Hole Spin with Gravitational Waves

Christian Adamcewicz^{1,2} , Shanika Galaudage^{3,4} , Paul D. Lasky^{1,2} , and Eric Thrane^{1,2} ¹ School of Physics and Astronomy, Monash University, Clayton VIC 3800, Australia; christian.adamcewicz@monash.edu² OzGrav: The ARC Centre of Excellence for Gravitational Wave Discovery, Clayton VIC 3800, Australia³ Université Côte d’Azur, Observatoire de la Côte d’Azur, CNRS, Laboratoire Lagrange, Bd de l’Observatoire, F-06304 Nice, France⁴ Université Côte d’Azur, Observatoire de la Côte d’Azur, CNRS, Artemis, Bd de l’Observatoire, F-06304 Nice, France

Received 2023 November 9; revised 2024 February 5; accepted 2024 February 25; published 2024 March 12

Abstract

Theoretical studies of angular momentum transport suggest that isolated stellar-mass black holes are born with negligible dimensionless spin magnitudes $\chi \lesssim 0.01$. However, recent gravitational-wave observations indicate $\gtrsim 40\%$ of binary black hole systems contain at least one black hole with a nonnegligible spin magnitude. One explanation is that the firstborn black hole spins up the stellar core of what will become the second-born black hole through tidal interactions. Typically, the second-born black hole is the “secondary” (less massive) black hole though it may become the “primary” (more massive) black hole through a process known as mass-ratio reversal. We investigate this hypothesis by analyzing data from the third gravitational-wave transient catalog using a “single-spin” framework in which only one black hole may spin in any given binary. Given this assumption, we show that at least 28% (90% credibility) of the LIGO–Virgo–KAGRA binaries contain a primary with significant spin, possibly indicative of mass-ratio reversal. We find no evidence for binaries that contain a secondary with significant spin. However, the single-spin framework is moderately disfavored (natural log Bayes factor $\ln \mathcal{B} = 3.1$) when compared to a model that allows both black holes to spin. If future studies can firmly establish that most merging binaries contain two spinning black holes, it may call into question our understanding of formation mechanisms for binary black holes or the efficiency of angular momentum transport in black hole progenitors.

Unified Astronomy Thesaurus concepts: [Black holes \(162\)](#); [Compact objects \(288\)](#); [Gravitational wave astronomy \(675\)](#); [Gravitational waves \(678\)](#)

1. Introduction

Recent works have suggested that angular momentum transport in black hole progenitors may be highly efficient, leading to slowly rotating stellar cores (Fuller & Ma 2019; Ma & Fuller 2019). As a result, their eventual core collapse should produce black holes with negligible dimensionless spin magnitudes $\chi \lesssim 0.01$ (Fuller & Ma 2019; Ma & Fuller 2019). However, studies of the merging binary black hole (BBH) population observed via gravitational waves have shown that $\gtrsim 40\%$ of systems contain at least one black hole with nonnegligible spin (Biscoveanu et al. 2021; Galaudage et al. 2021; Kimball et al. 2021; Roulet et al. 2021; Callister et al. 2022; Mould et al. 2022; Tong et al. 2022).

Tidal spin-up is a popular explanation for the nonnegligible spin observed in BBHs (Qin et al. 2018; Bavera et al. 2020; Belczynski et al. 2020; Olejak & Belczynski 2021; Fuller & Lu 2022; Hu et al. 2022; Ma & Fuller 2023). This scenario begins with an isolated binary, consisting of a black hole and a companion star that is the progenitor of the second-born black hole. The stellar companion’s envelope has been stripped through binary interactions, leaving behind a Wolf–Rayet star—a bare stellar core without an outer hydrogen envelope. The firstborn black hole induces tides on the Wolf–Rayet star that dissipate and produce a torque (Kushnir et al. 2017; Qin et al. 2018; Fuller & Lu 2022; Ma & Fuller 2023). As no outer layers

remain to carry away this angular momentum, the rotation is retained after core collapse.

The result is a BBH system with a rapidly rotating second-born black hole. Typically, the firstborn black hole forms the primary (more massive) black hole. However, if the binary undergoes mass-ratio reversal, the second-born (i.e., spinning) black hole will be the more massive component (Broekgaarden et al. 2022; Zevin & Bavera 2022). If the black holes seen with gravitational waves form in the field and are tidally spun up, we expect that only one black hole in any given binary should have nonnegligible spin. However, population models for BBH spins to date assume that each component’s spin is distributed independently relative to its companion’s (see, for example, Mould et al. 2022; Abbott et al. 2023b).

In this work, we model the population of merging BBH systems using a “single-spin” framework in which only one component in any given binary has nonnegligible spin. In doing so, we aim to ascertain whether tidal spin-up provides a good explanation for the spin properties of BBHs observed in gravitational waves. Within the single-spin framework, we seek to measure the fraction of mass-ratio reversed events with a spinning primary. The fraction of mass-ratio reversed mergers can vary significantly 0%–80% for different models (Broekgaarden et al. 2022; Zevin & Bavera 2022). Measuring the fraction of mass-ratio reversed mergers may therefore be useful for constraining binary evolution models.

The remainder of this work is structured as follows. We outline our population model and inference techniques in Section 2. In Section 3 we show the results of this analysis. We discuss the implications in Section 4.



Original content from this work may be used under the terms of the [Creative Commons Attribution 4.0 licence](#). Any further distribution of this work must maintain attribution to the author(s) and the title of the work, journal citation and DOI.

2. Method

We propose a spin model for the BBH population that builds on previous work from Galaudage et al. (2021) and Tong et al. (2022). It is a nested mixture model that allows for three subpopulations: binaries where neither black hole spins, binaries where the primary $i = 1$ black hole spins (but not the secondary $i = 2$), and binaries where the secondary spins (but not the primary). We refer to these three subpopulations as “nonspinning,” “primary-spinning,” and “secondary-spinning.” Note that in this framework, “nonspinning” is used as a proxy for a negligibly small spin $\chi_i \lesssim 0.01$ (indistinguishable from $\chi_i = 0$ with current measurement uncertainties; see Abbott et al. 2023a). This model does not allow for the primary and secondary black holes to both spin, but we return to this possibility below using a separate model. We assume the distribution of the two spin magnitudes χ_1 and χ_2 is

$$\begin{aligned} \pi(\chi_1, \chi_2 | \lambda_0, \lambda_1, \mu_\chi, \sigma_\chi^2) &= \lambda_0 \delta(\chi_1) \delta(\chi_2) + (1 - \lambda_0) \\ &\times (\lambda_1 \text{Beta}(\chi_1 | \mu_\chi, \sigma_\chi^2) \delta(\chi_2) + (1 - \lambda_1) \delta(\chi_1) \text{Beta}(\chi_2 | \mu_\chi, \sigma_\chi^2)). \end{aligned} \quad (1)$$

Here, $\delta(\chi_i)$ denotes the Dirac delta function, indicating a spin magnitude of zero. Following Wysocki et al. (2019), the nonzero spins are distributed according to a beta distribution with mean μ_χ and variance σ_χ^2 . This model assumes the $\chi_1 > 0$ subpopulation is identical to the $\chi_2 > 0$ subpopulation; the beta distributions for χ_1 and χ_2 have identical means and variances. One can allow these two distributions to be distinct, but we find that our results do not vary meaningfully if we allow for this possibility. The parameter λ_0 is the fraction of BBH systems with two nonspinning black holes. Within the remaining fraction $(1 - \lambda_0)$, λ_1 is the fraction with a primary-spinning black hole as opposed to a secondary.

Following Talbot & Thrane (2017), we model the (cosine) spin tilts $\cos t_i$ such that they are independently and identically distributed according to

$$\pi(\cos t_i | \sigma_t) = \mathcal{N}(\cos t_i | 1, \sigma_t) \Theta(\cos t_i + 1) \Theta(\cos t_i - 1), \quad (2)$$

where \mathcal{N} is a normal distribution with a mean of 1 and width σ_t , and Θ is a Heaviside step function—truncating the distribution to lie between $\cos t_i \in [-1, 1]$. This model is congruent with the assumption that spinning systems are tidally spun up and thus should have preferentially aligned spins (e.g., Ma & Fuller 2023).⁵ We simultaneously fit the mass and redshift distributions using the POWER-LAW + PEAK mass model from Talbot & Thrane (2018) and the POWER-LAW redshift model from Fishbach et al. (2018).

We account for mass and redshift-based selection effects (see Messenger & Veitch 2013; Abbott et al. 2019; Thrane & Talbot 2019; Abbott et al. 2021, 2023b) using the injection set from LIGO-Virgo-KAGRA (LVK; LVK 2023) collaboration (see Tiwari 2018; Farr 2019; Mandel et al. 2019). However, we do not include spin-based effects due to sampling issues that

arise at values of $\chi_i \approx 0$.⁶ These spin-based selection effects are believed to be relatively small for populations with less than ~ 100 events (Ng et al. 2018; Abbott et al. 2023b). Furthermore, these effects manifest as a bias away from effective inspiral spins $\chi_{\text{eff}} < 0$, as well as larger uncertainties on the spin properties of $\chi_{\text{eff}} < 0$ systems (Ng et al. 2018). We do not expect any correlations between such systems and the tendency to be primary or secondary spinning and thus do not expect these effects to significantly bias our results. To test this, we draw 10^5 events from our model, inject the corresponding signals into simulated design-sensitivity LIGO noise, and find the fraction of injections that are recovered with an optimal network signal-to-noise ratio > 11 . We carry out this calculation four times: assuming only primary-spin, assuming only secondary-spin, assuming both-spin, and assuming no-spin populations. We find that the fraction of above-detection-threshold events varies by $\lesssim 0.1\%$ between each subpopulation. This supports our expectation that the results will not change significantly when we include spin-based selection effects.

We perform hierarchical Bayesian inference in order to measure the population hyperparameters using gravitational-wave data from LVK (Aasi et al. 2015; Acernese et al. 2015; Akutsu et al. 2021).⁷ We do so using the nested sampler DYNESTY (Speagle 2020) inside of the GWPopulation (Talbot et al. 2019) package, which itself is built on top of Bilby (Ashton et al. 2019; Romero-Shaw et al. 2020). Our data set begins with the 69 BBH observations from the third LVK gravitational-wave transient catalog (GWTC-3; Abbott et al. 2023a) that were considered reliable for population analyses (events with a false alarm rate $< 1 \text{ yr}^{-1}$; Abbott et al. 2023b). However, we omit two events, GW191109_010717 and GW200129_065458, due to concerns related to data quality (Davis et al. 2022; Payne et al. 2022; Macas & Lundgren 2023; H. Tong 2023, private communication), so we analyze 67 BBH events. We find that the inclusion of these two events does not drastically change our results (see Section 3).

For each BBH event, we perform three sets of parameter estimation to be used in our hierarchical inference: once with a no-spin prior $\chi_1 = \chi_2 = 0$, once with a primary-spin prior $\chi_2 = 0$, and once with a secondary-spin prior $\chi_1 = 0$. Whichever black hole is allowed to spin is sampled with a prior that is uniform in χ_i . We use the IMRPhenomXPHM waveform model (Pratten et al. 2021). Carrying out three suites of parameter estimation runs allows us to avoid potential issues of undersampling the posterior distribution near $\chi_i = 0$ during hierarchical inference (see Appendix A, as well as Galaudage et al. 2021; Tong et al. 2022; Adamcewicz et al. 2023, for more details).

In order to compare the single-spin hypothesis to the hypothesis that both black holes may spin, we also construct and fit a “both-spin” population model. This consists of the EXTENDED model for spin magnitude from Tong et al. (2022; see their Equation (2)), combined with our simplified model for spin orientation defined in Equation (2). We obtain a fourth set of parameter estimation results in which both black holes may have nonzero spins in order to perform hierarchical inference with this both-spin population model.

⁵ Further tests that allow the mean of the spin tilt distributions to vary allow $\cos t_1$ and $\cos t_2$ to be distributed independently or allow for an isotropic subpopulation (as per Talbot & Thrane 2017) suggest that our conclusions do not depend strongly on the model for spin orientation (see also Mould et al. 2022; Tong et al. 2022; Vitale et al. 2022).

⁶ Significant code development is required to implement spin-based selection effects.

⁷ For a review on parameter estimation and hierarchical inference in gravitational-wave astronomy, we point the reader to Thrane & Talbot (2019).

We set uniform priors over $[0, 1]$ for the mixing fractions λ_0 and λ_1 . The priors on other population hyperparameters are identical to those used in Tong et al. (2022). These priors do not allow for singularities in the χ_i beta distributions.

3. Results

First, we compare the evidence for the “single-spin” population model proposed in Section 2 to the previously used “both-spin” model in which both black holes in any given binary may spin. We find that the single-spin model is disfavored by a natural log Bayes factor of $\ln \mathcal{B} = 3.1$ (difference in maximum natural log likelihood of $\Delta \ln \mathcal{L}_{\max} = 2.0$). The single-spin model incurs an Occam penalty for its added complexity relative to the both-spin model, which does not have the λ_1 parameter. However, the both-spin model also yields a better overall fit, evident by its larger maximum likelihood. The numerical value of $\ln \mathcal{B} = 3.1$ is not large enough to draw a strong conclusion that the both-spin model is clearly preferred over the single-spin model.⁸ It is, however, an interesting preliminary result that we are keen to revisit as more data become available. When including GW191109_010717 and GW200129_065458 (or either event on its own), we find that support for the both-spin model increases by $\Delta \ln \mathcal{B} \lesssim 1$.

Next, we set aside for a moment the possibility that both black holes have nonnegligible spin and assume that spinning black holes are tidally spun up (i.e., that there can be at most one black hole with nonnegligible spin in each binary). In Figure 1, we show the posterior corner plot for the mixing fractions λ_0 (the fraction of events with nonnegligible spin) and λ_1 (the fraction of spinning events with $\chi_1 > 0$ as opposed to $\chi_2 > 0$). We show posterior distributions for other population hyperparameters governing BBH spins in Appendix B. With 90% credibility, we measure the fraction of nonspinning systems to be $\lambda_0 \leq 0.60$ —consistent with the results of Tong et al. (2022). Among BBH systems with measurable component spins, we find the fraction of primary-spinning systems to be $\lambda_1 \geq 0.59$ (90% credibility). We rule out $\lambda_1 = 0$ with high credibility. The posterior is peaked at $\lambda_1 = 1$, the point in parameter space where no secondary black holes have appreciable spin. These results do not change meaningfully when including GW191109_010717, GW200129_065458, or both.

As a check, we analyze 10 simulated signals with $\chi_1 = 0$ and $\chi_2 > 0$ drawn from a beta distribution. As expected, the resulting posterior from hierarchical inference peaks at $(\lambda_0 = 0, \lambda_1 = 0)$, which assures us that our result does not arise from some pathological prior effect.

It is useful to understand which features in the data are most responsible for our results. In Figure 2, we plot the evidence obtained during the initial parameter estimation for each event, given each different spin hypothesis (see Section 2 and Appendix A for how these evidence values are used in the hierarchical analysis presented above). In this scatterplot, the horizontal axis is the natural log Bayes factor comparing the

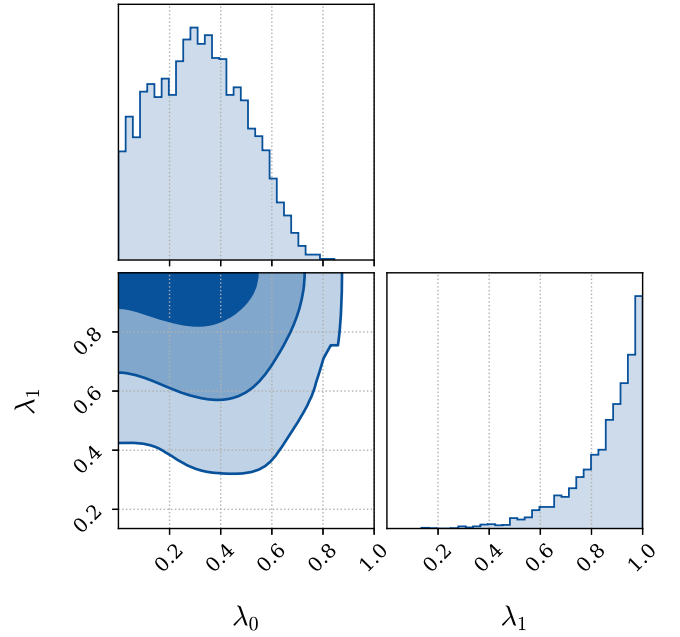


Figure 1. Posterior corner plot for the fraction of BBH systems with negligible spin λ_0 and the fraction of spinning BBH systems with $\chi_1 > 0$, λ_1 . The different shades indicate the 50%, 90%, and 99% credible intervals. The fact that $\lambda_0 = 1$ is ruled out is already well established: at least some BBH systems contain a black hole with nonnegligible spin. The fact that $\lambda_1 = 0$ is ruled out suggests that—within the single-spin framework and among binaries with a spinning black hole—it is the primary mass black hole that is spinning at least 59% of the time. Under the assumption of single spin, the data are consistent with the possibility that only the primary black hole spins.

primary-spin evidence \mathcal{Z}_1 to the secondary-spin evidence \mathcal{Z}_2 :

$$\ln \mathcal{B}_{\text{primary}} = \ln \left(\frac{\mathcal{Z}_1}{\mathcal{Z}_2} \right). \quad (3)$$

The vertical axis is the natural log Bayes factor comparing the single-spin evidence (\mathcal{Z}_1 or \mathcal{Z}_2 —whichever is larger) to the both-spinning evidence \mathcal{Z}_b :

$$\ln \mathcal{B}_{\text{single}} = \ln \left(\frac{\max(\mathcal{Z}_1, \mathcal{Z}_2)}{\mathcal{Z}_b} \right). \quad (4)$$

Meanwhile, the color bar shows the natural log Bayes factor comparing the spinning hypothesis (whichever is largest) to the no-spin hypothesis:

$$\ln \mathcal{B}_{\text{spin}} = \ln \left(\frac{\max(\mathcal{Z}_1, \mathcal{Z}_2, \mathcal{Z}_b)}{\mathcal{Z}_0} \right). \quad (5)$$

Events with evidence for spin (blue dots) show a small preference to lie below zero in the vertical axis, indicating a preference for the both-spin hypothesis. This amalgamates as a moderate preference for both-spin systems over single-spin systems on a population level ($\ln \mathcal{B} = 3.1$ from above). These events tend to show a much larger deviation from zero in the horizontal axis—trending toward values of $\ln \mathcal{B}_{\text{primary}} > 0$, indicating a preference for primary-spin as opposed to secondary-spin. The events that prefer secondary-spin over primary-spin ($\ln \mathcal{B}_{\text{primary}} < 0$) tend to be white circles, indicating that these events are best explained as not spinning at all. Under the assumption of single-spin, this results in a strong

⁸ We find that we can draw the same conclusion when including single-spin and both-spin binaries in the same population model: a dominant subpopulation of secondary-spin black holes is ruled out, while both-spin binaries are modestly preferred over primary-spin-only systems. Due to an Occam penalty, this model is disfavored when compared to the simpler both-spin model by a natural log Bayes factor $\ln \mathcal{B} = 1.2$. No noteworthy covariance in mixing fractions arises within this framework.

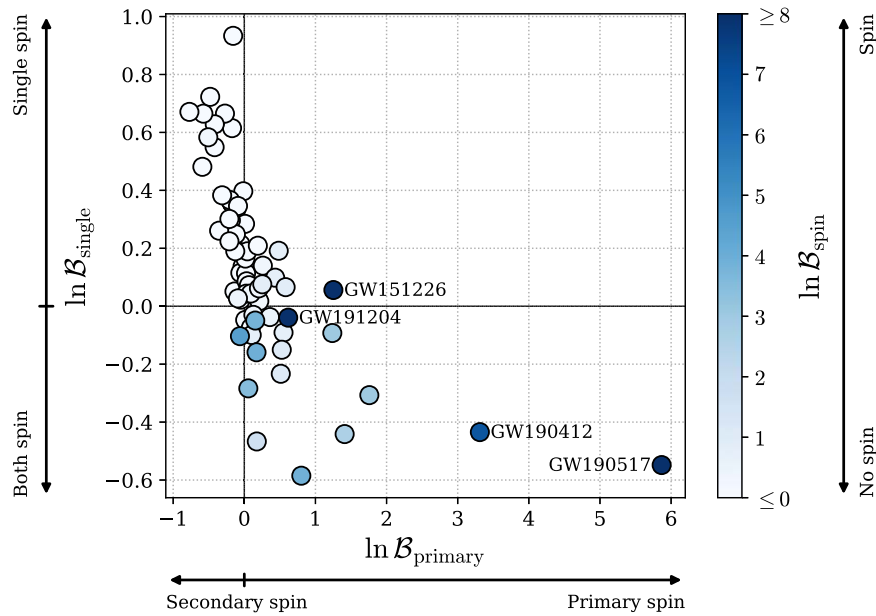


Figure 2. A comparison of each spin hypothesis for each event. Each point represents a single BBH event observed in gravitational waves. The color of the point represents the natural log Bayes factor for the spinning hypothesis $\ln \mathcal{B}_{\text{spin}}$; white circles are events best explained as nonspinning, while blue circles are best explained as containing at least one spinning black hole. The vertical axis shows the natural log Bayes factor comparing the single-spin hypothesis (positive values) to the both-spin hypothesis (negative values) $\ln \mathcal{B}_{\text{single}}$. The horizontal axis shows the natural log Bayes factor comparing the primary-spin hypothesis (positive values) to the secondary-spin hypothesis (negative values) $\ln \mathcal{B}_{\text{primary}}$. Note there is significantly less spread in $\mathcal{B}_{\text{single}}$ than there is in $\mathcal{B}_{\text{primary}}$, indicating that it is relatively difficult to ascertain if the primary is spinning by itself. The four events with the highest evidence for spin (darkest blue) are labeled, being GW190412_053044, GW190517_055101, GW151226, and GW191204_171526.

preference for primary-spin systems on the population level, as seen in Figure 1.

4. Discussion

We find that the spin properties of the BBHs in GWTC-3 require at least 28% of all binaries to include a primary with nonnegligible spin. Among spinning binaries, we find that at least 59% of systems have a nonnegligible primary spin. These binaries are either mass-ratio reversed or contain two black holes with nonnegligible spin.

This result is consistent with predictions from Zevin & Bavera (2022) and Broekgaarden et al. (2022), which suggest that up to $\approx 72\%$ – 82% of the BBH population may be mass-ratio reversed. Furthermore, Farah et al. (2024) find that a large fraction of the BBH population is consistent with mass-ratio reversal due to asymmetries in the distributions of primary and secondary masses. While our posterior for the fraction of primary-spinning systems λ_1 is consistent with 0.82, it peaks at $\lambda_1 = 1$. With additional events, it may be possible in the near future to distinguish between $\lambda_1 = 0.80$ and $\lambda_1 = 1$. A strong preference for $\lambda_1 = 1$ would be difficult to explain within the standard field formation scenario given our current understanding of angular momentum transport and tidal spin-up (see Qin et al. 2018; Fuller & Ma 2019; Ma & Fuller 2023, for example). Of course, if a strong statistical preference for the both-spinning framework can be established, then the entire discussion of mass-ratio reversal may be moot. It would be difficult to explain such a result within the field binary framework unless angular momentum transport in massive stars is less efficient than expected (see Heger et al. 2005; Qin et al. 2018; Fuller & Ma 2019, and discussions therein). On this point, Callister et al. (2021) find that if spinning BBHs are formed in the field and undergo tidal spin-up, extreme natal kicks are required to produce the observed range of spin tilts in

the LVK data. Callister et al. (2021) suggest that inefficient angular momentum transport in black hole progenitors (thus nonnegligible spins for firstborn black holes) may alleviate this requirement for extreme kicks. This is because the firstborn black hole forms when the binary has a greater orbital separation so is more easily misaligned by smaller natal kicks (Callister et al. 2021). However, these findings are disputed by Stevenson (2022), who questions the assumption that all secondary-mass black holes can be tidally spun up.

Qin et al. (2022) highlights the BBH merger GW190403_051519: an event that does not pass the threshold for inclusion in population studies yet has the highest inferred effective inspiral spin of any LVK observation to date, $\chi_{\text{eff}} \approx 0.7$. This event, if authentic, provides a strong signature for a rapidly spinning primary $\chi_1 = 0.92^{+0.07}_{-0.22}$, making it consistent with the results presented here.

The event GW190412_53044 shows the second strongest evidence for a primary-spin component in our analyses. Motivated by the tidal spin-up hypothesis, Mandel & Fragos (2020) suggest that GW190412_53044 can be explained as a system with a rapidly rotating secondary by imposing a prior in which the primary is assumed to have negligible spin. However, Zevin et al. (2020) argue that this assumption is statistically disfavored by the data—a point that we reiterate in Figure 2.

We come to a similar conclusion as Mould et al. (2022), in that both studies suggest that both black holes spinning in any given binary is the best description for the majority of the population. Mould et al. (2022) suggest that such systems make up $\approx 77\%$ of BBHs. However, Mould et al. (2022) find that a larger fraction of BBH systems may be described as secondary-spinning ($\lesssim 42\%$) as opposed to primary-spinning ($\lesssim 32\%$). In contrast, setting aside the possibility that both black holes may spin, our results suggest that a much larger

fraction of BBH systems can be described as primary-spinning ($\lesssim 88\%$) as opposed to secondary-spinning ($\lesssim 28\%$). While our inferences on these fractions may decrease when a both-spin subpopulation is factored in, the relative proportion of primary-spin to secondary-spin systems does not vary meaningfully. Furthermore, the results of Mould et al. (2022) suggest that $\lesssim 6\%$ of binaries can be described with both black holes having negligible spins, while we measure this fraction to be $\lesssim 60\%$. Our results, however, are consistent with the findings of Callister et al. (2022), Tong et al. (2022), and Roulet et al. (2021) on this front. These discrepancies may be due to a number of factors. First, our spin models are set up to explicitly test the hypothesis that only one black hole spins in any given binary, whereas Mould et al. (2022) endeavor to measure the distributions of χ_1 and χ_2 independently, without attempting to force one or more spin magnitudes to zero in each binary. Also, Mould et al. (2022) do not use dedicated samples near $\chi_i \approx 0$, which may lead to issues of undersampling this region.

Another possibility is that a large fraction of the events in GWTC-3 ($\gtrsim 28\%$) is not formed in the field (Zevin et al. 2021). Binaries merging in dense stellar environments can merge repeatedly through hierarchical mergers (e.g., Fishbach et al. 2017; Gerosa & Berti 2017; Rodriguez et al. 2019; Doctor et al. 2020, 2021). While many analyses suggest that the LVK data are consistent with isotropy in BBH spin tilts (Callister et al. 2022; Vitale et al. 2022; Abbott et al. 2023b; Callister & Farr 2023; Edelman et al. 2023; Golomb & Talbot 2023), other studies have found that BBH spin may tend toward alignment with the orbital angular momentum (e.g., Galadage et al. 2021; Roulet et al. 2021; Tong et al. 2022). If it is true that BBH spins are preferentially aligned, this would conflict with what one would expect for binaries formed in globular clusters (Rodriguez et al. 2016; Farr et al. 2017; Stevenson et al. 2017; Talbot & Thrane 2017; Vitale et al. 2017; Yu et al. 2020).

Active galactic nuclei (AGNs) may provide an environment in which both black holes can be spun up (through both accretion and hierarchical mergers) while providing a preferred axis with which to align black hole spin (Bogdanović et al. 2007; Vajpeyi et al. 2022; McKernan & Ford 2023). Namely, prograde accretion of gas in AGN disks may simultaneously spin up merging black holes (primary or secondary) and torque them into alignment with the disk’s rotation (Bogdanović et al. 2007; McKernan & Ford 2023). At the same time, the high stellar densities and escape velocities of AGNs provide a suitable environment for potential hierarchical mergers, producing black holes with $\chi_i \approx 0.7$ (see, for example, Tichy & Marronetti 2008)—and large masses like the components of GW190521 (Abbott et al. 2020a, 2020b). These black holes may then be spun down to magnitudes consistent with gravitational-wave observations ($\chi_i \approx 0.2\text{--}0.4$) via retrograde accretion of gas in the AGN disk (McKernan & Ford 2023).

Black holes observed in high-mass X-ray binaries (with lower-mass companions) appear to have large aligned spins $\chi_1 \gtrsim 0.8$ (Liu et al. 2008; Miller-Jones et al. 2021; Reynolds 2021), often thought to be a result of accretion (Podsiadlowski et al. 2003; Qin et al. 2019; Shao & Li 2020).⁹ If primary-spin systems are common in gravitational waves, this may indicate that merging BBHs can undergo a similar

evolutionary process to high-mass X-ray binaries (Fishbach & Kalogera 2022; Gallegos-Garcia et al. 2022; Shao & Li 2022). Assuming that case-A mass transfer is responsible for spinning up the primary, Gallegos-Garcia et al. (2022) find that up to $\approx 20\%$ of BBH mergers may be former high-mass X-ray binaries. However, previous studies show that the large spin magnitudes of black holes in high-mass X-ray binaries are in tension with the BBH spin distribution from gravitational waves (Roulet & Zaldarriaga 2019; Fishbach & Kalogera 2022). This tension may be somewhat relieved when modeling the BBH population under the assumption of rapidly spinning primaries (Fishbach & Kalogera 2022). On this note, we find increased support for large spin magnitudes when using the single-spin framework (see Figure 3 from Appendix B). We find that the single-spin framework allows for up to $\approx 10\%$ of BBHs to have $\chi_i \geq 0.8$, while the (preferred) both-spin model suggests these systems may only make up $\lesssim 3\%$ of the population (90% credibility). This is most likely driven by support for high values of χ_{eff} in the data (predominantly from the dark blue events in Figure 2). When only one black hole is allowed to spin, higher spin magnitudes are required to reach these large values of χ_{eff} when compared to the scenario in which both black holes may spin.

Acknowledgments

We thank our anonymous reviewer, Amanda Farah, Christopher P. L. Berry, Sylvia Biscoveanu, Thomas Callister, Maya Fishbach, Matthew Mould, and Salvatore Vitale for helpful comments on this manuscript. We acknowledge support from the Australian Research Council (ARC) Centre of Excellence CE170100004, LE210100002, and ARC DP230103088. This material is based upon work supported by NSF’s LIGO Laboratory which is a major facility fully funded by the National Science Foundation. The authors are grateful for computational resources provided by the LIGO Laboratory and supported by National Science Foundation Grants PHY-0757058 and PHY-0823459.

This research has made use of data or software obtained from the Gravitational Wave Open Science Center (<http://www.gw-openscience.org>), a service of LIGO Laboratory, the LIGO Scientific Collaboration, the Virgo Collaboration, and KAGRA. LIGO Laboratory and Advanced LIGO are funded by the United States National Science Foundation (NSF) as well as the Science and Technology Facilities Council (STFC) of the United Kingdom, the Max-Planck-Society (MPS), and the State of Niedersachsen/Germany for support of the construction of Advanced LIGO and construction and operation of the GEO600 detector. Additional support for Advanced LIGO was provided by the Australian Research Council. Virgo is funded, through the European Gravitational Observatory (EGO), by the French Centre National de Recherche Scientifique (CNRS), the Italian Istituto Nazionale di Fisica Nucleare (INFN) and the Dutch Nikhef, with contributions by institutions from Belgium, Germany, Greece, Hungary, Ireland, Japan, Monaco, Poland, Portugal, Spain. The construction and operation of KAGRA are funded by Ministry of Education, Culture, Sports, Science and Technology (MEXT), and Japan Society for the Promotion of Science (JSPS), National Research Foundation (NRF) and Ministry of Science and ICT (MSIT) in Korea, Academia Sinica (AS) and the Ministry of Science and Technology (MoST) in Taiwan.

⁹ However, these measurements may be affected by systematic uncertainties, resulting in errors on the order of $\chi_1 \sim 0.1$ (Taylor & Reynolds 2018; Salvesen & Miller 2020; Falanga et al. 2021).

Appendix A Population Likelihoods with Sharp Features

When introducing sharp features (like a nonspinning peak) into a population model, one can encounter issues of under-sampling during hierarchical inference. That is to say, an insufficient number of fiducial (event-level) samples in the relevant region of parameter space makes the sharp feature in the population model difficult to resolve via reweighting. This may lead to spurious inferences.

To counteract this, we use the method presented in Galadage et al. (2021), Tong et al. (2022), and Adamcewicz et al. (2023). Each variation of the zero-spin peak (no-spin $\chi_1 = \chi_2 = 0$, primary-spin $\chi_2 = 0$, and secondary-spin $\chi_1 = 0$; see Section 2) is imposed on the prior during separate event-level parameter estimation analyses (reiterating, wherever $\chi_i > 0$, the prior is uniform). In effect, this means that there is an abundance of samples within each variation of the zero-spin peak and spin samples only require reweighting outside of these sharp features (when $\chi_i > 0$).

Using these three sets of parameter estimation results, we can construct a population likelihood following the model from Section 2 as

$$\begin{aligned} \mathcal{L}(d|\Lambda, \lambda_0, \lambda_1) &= \prod_i^N \frac{1}{n} \left[\lambda_0 \mathcal{Z}_0^i \sum_k^n w_0(\theta_k^i|\Lambda) + (1 - \lambda_0) \right. \\ &\times \left. \left(\lambda_1 \mathcal{Z}_1^i \sum_k^n w_1(\theta_k^i|\Lambda) + (1 - \lambda_1) \mathcal{Z}_2^i \sum_k^n w_2(\theta_k^i|\Lambda) \right) \right]. \end{aligned} \quad (\text{A1})$$

Here, λ_0 and λ_1 are the mixing fractions for different spin configurations (see Section 2), Λ denotes the set of all other population hyperparameters (e.g., μ_χ and σ_χ^2), N is the number of events, and n is the total number of samples per event obtained from parameter estimation. The Bayesian

evidence obtained during parameter estimation for event i , with spin configuration s (no-spin $s = 0$, primary-spin $s = 1$, and secondary-spin $s = 2$) is denoted \mathcal{Z}_s^i . Finally, the weight w_s for a given parameter estimation sample θ_k^i is

$$w_s(\theta|\Lambda) = \frac{\pi_s(\chi_1, \chi_2, \cos t_1, \cos t_2|\Lambda) \pi(m_1, q, z|\Lambda)}{\pi(\chi_1, \chi_2, \cos t_1, \cos t_2, m_1, q, z|\emptyset)}, \quad (\text{A2})$$

where $\pi(\theta|\emptyset)$ is the prior probability from parameter estimation, $\pi(m_1, q, z|\Lambda)$ is the population model for primary mass, mass ratio, and redshift from Section 2, and

$$\pi_0(\chi_1, \chi_2, \cos t_1, \cos t_2|\Lambda) = \delta(\chi_1) \delta(\chi_2), \quad (\text{A3})$$

$$\begin{aligned} \pi_1(\chi_1, \chi_2, \cos t_1, \cos t_2|\Lambda) \\ = \text{Beta}(\chi_1|\mu_\chi, \sigma_\chi^2) \delta(\chi_2) \pi(\cos t_1|\sigma_t), \end{aligned} \quad (\text{A4})$$

$$\begin{aligned} \pi_2(\chi_1, \chi_2, \cos t_1, \cos t_2|\Lambda) \\ = \delta(\chi_1) \text{Beta}(\chi_2|\mu_\chi, \sigma_\chi^2) \pi(\cos t_2|\sigma_t) \end{aligned} \quad (\text{A5})$$

give the spin model for each configuration. Again, note that only the uniformly sampled $\chi_i > 0$ spin values are reweighted (to follow a beta distribution). Also note that we have omitted the detection efficiency factor that accounts for selection effects from Equation (A1) for the sake of brevity.

Appendix B Additional Plots

We include an additional corner plot for the remaining population hyperparameters governing the BBH spin distribution for the single-spin and both-spin models in Figure 3. We also plot population predictive distributions (for both models) for spin magnitudes and tilts in Figures 4 and 5 respectively.

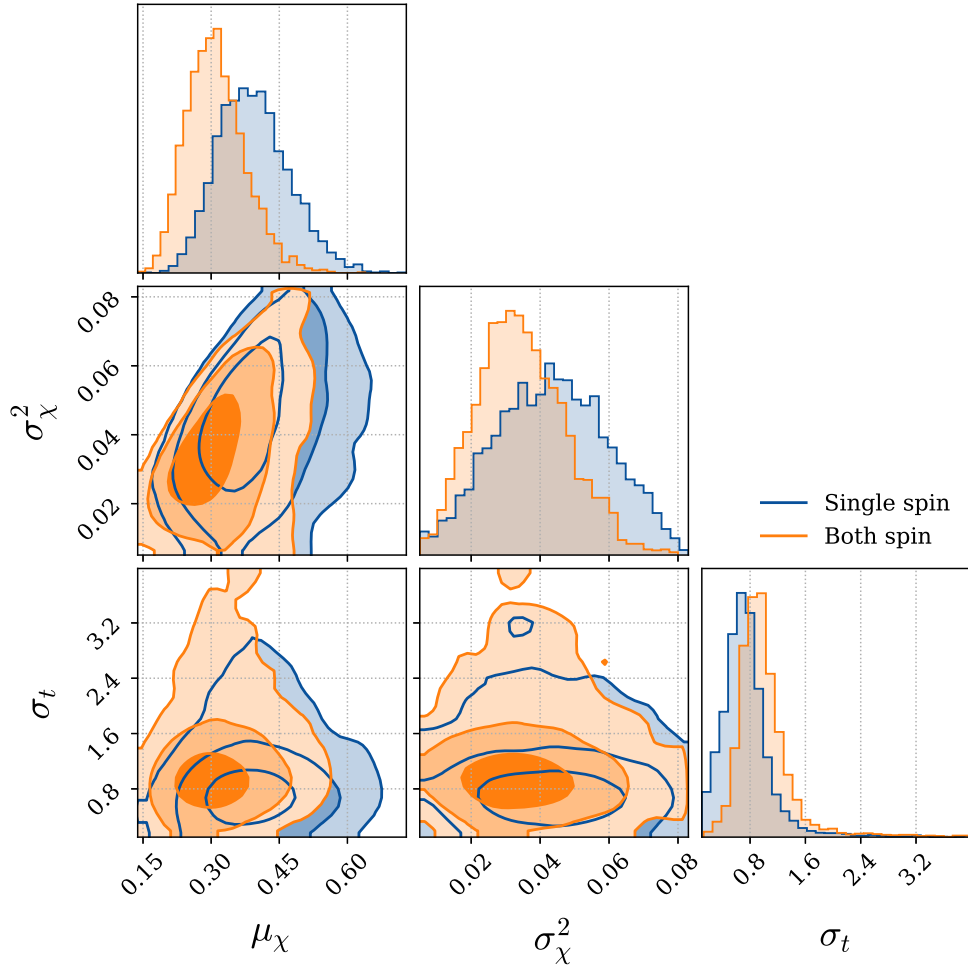


Figure 3. Posterior corner plot for hyperparameters governing the BBH spin distribution. Blue shows the posteriors given the single-spin model (Equation (1)), while orange shows the posteriors given the both-spin model (Equation (2) from Tong et al. 2022). Both models use Equation (2) for spin orientation. Contours on the two-dimensional plot give the 50%, 90%, and 99% credible regions. In the single-spin framework, we measure the mean and variance of the spin magnitude distribution to be $\mu_\chi = 0.39^{+0.14}_{-0.11}$ and $\sigma_\chi^2 = 0.04^{+0.03}_{-0.03}$, respectively. Meanwhile, the width of the cosine spin tilt distribution is found to be $\sigma_t = 0.70^{+0.64}_{-0.44}$. In the both-spin framework, we find the mean and variance of the spin magnitude distribution to be $\mu_\chi = 0.31^{+0.12}_{-0.09}$ and $\sigma_\chi^2 = 0.03^{+0.02}_{-0.02}$, with the width of the cosine spin tilt distribution being $\sigma_t = 0.93^{+0.73}_{-0.39}$.

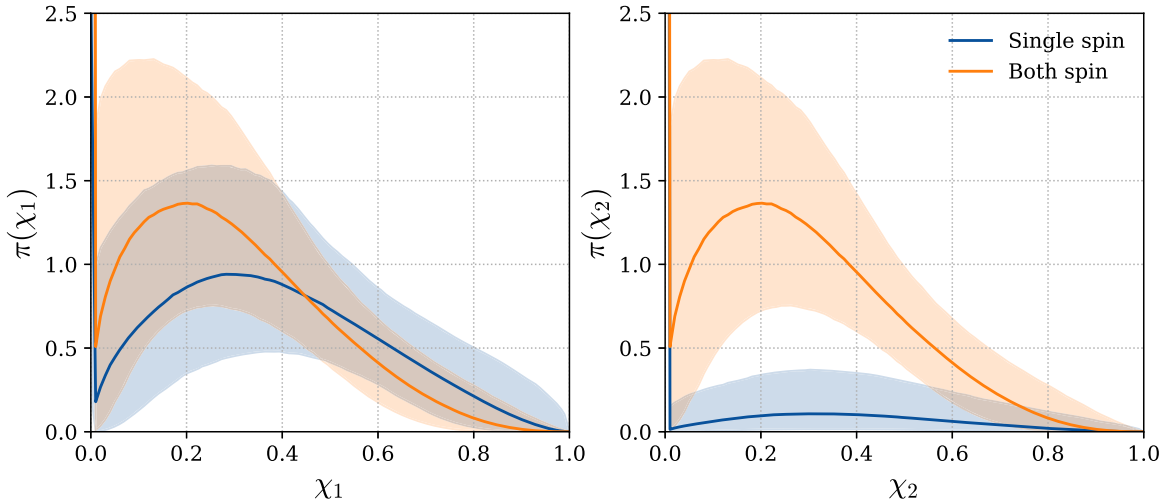


Figure 4. Population predictive distributions for primary (left) and secondary (right) spin magnitude. Blue shows the single-spin model (Equation (1)), while orange shows the both-spin model (Equation (2) from Tong et al. 2022). In either model the distributions for nonzero χ_1 and χ_2 must have identical shapes. In the both-spin model, they must also have identical amplitudes. The both-spin model enforces that either $\chi_1 = \chi_2 = 0$ or that $\chi_1 > 0$ and $\chi_2 > 0$ simultaneously. Meanwhile, the single-spin model enforces that $\chi_1 = \chi_2 = 0$, that $\chi_1 > 0$ and $\chi_2 = 0$, or that $\chi_1 = 0$ and $\chi_2 > 0$.

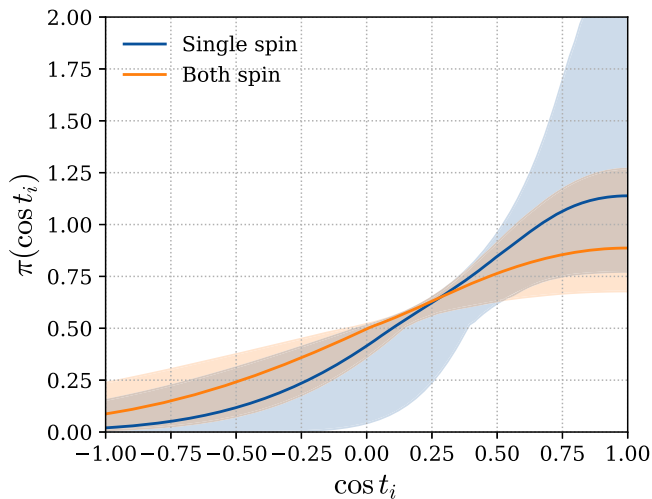



Figure 5. Population predictive distributions for cosine spin tilts following Equation (2). Blue shows the results for the single-spin model (Equation (1)), while orange shows the results for the both-spin model (Equation (2)) from Tong et al. (2022).

ORCID iDs

Christian Adamcewicz  <https://orcid.org/0000-0001-5525-6255>

Shanika Galadage  <https://orcid.org/0000-0002-1819-0215>

Paul D. Lasky  <https://orcid.org/0000-0003-3763-1386>

Eric Thrane  <https://orcid.org/0000-0002-4418-3895>

References

- Aasi, J., Abbott, B. P., Abbott, R., et al. 2015, *CQGra*, 32, 074001
- Abbott, B. P., Abbott, R., Abbott, T. D., et al. 2019, *ApJL*, 882, L24
- Abbott, R., Abbott, T. D., Abraham, S., et al. 2020a, *PhRvL*, 125, 101102
- Abbott, R., Abbott, T. D., Abraham, S., et al. 2020b, *ApJL*, 900, L13
- Abbott, R., Abbott, T. D., Abraham, S., et al. 2021, *ApJL*, 913, L7
- Abbott, R., Abbott, T. D., Acernese, F., et al. 2023a, *PhRvX*, 13, 041039
- Abbott, R., Abbott, T. D., Acernese, F., et al. 2023b, *PhRvX*, 13, 011048
- Acernese, F., Agathos, M., Agatsuma, K., et al. 2015, *CQGra*, 32, 024001
- Adamcewicz, C., Lasky, P. D., & Thrane, E. 2023, *ApJ*, 958, 13
- Akutsu, T., Ando, M., Arai, K., et al. 2021, *PTEP*, 2021, 05A101
- Ashton, G., Hübner, M., Lasky, P. D., et al. 2019, *ApJS*, 241, 27
- Bavera, S. S., Fragos, T., Qin, Y., et al. 2020, *A&A*, 635, A97
- Belczynski, K., Klencki, J., Fields, C. E., et al. 2020, *A&A*, 636, A104
- Biscoveanu, S., Isi, M., Vitale, S., & Varma, V. 2021, *PhRvL*, 126, 171103
- Bogdanović, T., Reynolds, C. S., & Miller, M. C. 2007, *ApJL*, 661, L147
- Broekgaarden, F. S., Stevenson, S., & Thrane, E. 2022, *ApJ*, 938, 45
- Callister, T. A., & Farr, W. M. 2023, arXiv:2302.07289
- Callister, T. A., Farr, W. M., & Renzo, M. 2021, *ApJ*, 920, 157
- Callister, T. A., Miller, S. J., Chatzioannou, K., & Farr, W. M. 2022, *ApJL*, 937, L13
- Davis, D., Littenberg, T. B., Romero-Shaw, I. M., et al. 2022, *CQGra*, 39, 245013
- Doctor, Z., Farr, B., & Holz, D. E. 2021, *ApJL*, 914, L18
- Doctor, Z., Wysocki, D., O’Shaughnessy, R., Holz, D. E., & Farr, B. 2020, *ApJ*, 893, 35
- Edelman, B., Farr, B., & Doctor, Z. 2023, *ApJ*, 946, 16
- Falanga, M., Bakala, P., Placa, R. L., et al. 2021, *MNRAS*, 504, 3424
- Farah, A. M., Fishbach, M., & Holz, D. E. 2024, *ApJ*, 962, 89
- Farr, W. M. 2019, *RNAAS*, 3, 66
- Farr, W. M., Stevenson, S., Miller, M. C., et al. 2017, *Natur*, 548, 426
- Fishbach, M., Holz, D. E., & Farr, B. 2017, *ApJL*, 840, L24
- Fishbach, M., Holz, D. E., & Farr, W. M. 2018, *ApJL*, 863, L41
- Fishbach, M., & Kalogera, V. 2022, *ApJL*, 929, L26
- Fuller, J., & Lu, W. 2022, *MNRAS*, 511, 3951
- Fuller, J., & Ma, L. 2019, *ApJL*, 881, L1
- Galadage, S., Talbot, C., Nagar, T., et al. 2021, *ApJL*, 921, L15
- Gallegos-Garcia, M., Fishbach, M., Kalogera, V., Berry, C. P. L., & Doctor, Z. 2022, *ApJL*, 938, L19
- Gerosa, D., & Berti, E. 2017, *PhRvD*, 95, 124046
- Golomb, J., & Talbot, C. 2023, *PhRvD*, 108, 103009
- Heger, A., Woosley, S. E., & Spruit, H. C. 2005, *ApJ*, 626, 350
- Hu, R.-C., Zhu, J.-P., Qin, Y., et al. 2022, *ApJ*, 928, 163
- Kimball, C., Talbot, C., Berry, C. P. L., et al. 2021, *ApJL*, 915, L35
- Kushnir, D., Zaldarriaga, M., Kollmeier, J. A., & Waldman, R. 2017, *MNRAS*, 467, 2146
- Liu, J., McClintock, J. E., Narayan, R., Davis, S. W., & Orosz, J. A. 2008, *ApJL*, 679, L37
- LVK 2023, Compact Binary Coalescences Observed by LIGO and Virgo During the Third Observing Run ? O1+O2+O3 Search Sensitivity Estimates, v2, Zenodo, doi:10.5281/zenodo.7890398
- Ma, L., & Fuller, J. 2019, *MNRAS*, 488, 4338
- Ma, L., & Fuller, J. 2023, *ApJ*, 952, 53
- Macas, R., & Lundgren, A. 2023, *PhRvD*, 108, 063016
- Mandel, I., Farr, W. M., & Gair, J. R. 2019, *MNRAS*, 486, 1086
- Mandel, I., & Fragos, T. 2020, *ApJL*, 895, L28
- McKernan, B., & Ford, K. E. S. 2023, arXiv:2309.15213
- Messenger, C., & Veitch, J. 2013, *NJPh*, 15, 053027
- Miller-Jones, J. C. A., Bahramian, A., Orosz, J. A., et al. 2021, *Sci*, 371, 1046
- Mould, M., Gerosa, D., Broekgaarden, F. S., & Steinle, N. 2022, *MNRAS*, 517, 2738
- Ng, K. K., Vitale, S., Zimmerman, A., et al. 2018, *PhRvD*, 98, 083007
- Olejak, A., & Belczynski, K. 2021, *ApJL*, 921, L2
- Payne, E., Hourihane, S., Golomb, J., et al. 2022, *PhRvD*, 106, 104017
- Podsiadlowski, P., Rappaport, S., & Han, Z. 2003, *MNRAS*, 341, 385
- Pratten, G., García-Quiros, C., Colleoni, M., et al. 2021, *PhRvD*, 103, 104056
- Qin, Y., Fragos, T., Meynet, G., et al. 2018, *A&A*, 616, A28
- Qin, Y., Marchant, P., Fragos, T., Meynet, G., & Kalogera, V. 2019, *ApJL*, 870, L18
- Qin, Y., Wang, Y.-Z., Wu, D.-H., Meynet, G., & Song, H. 2022, *ApJ*, 924, 129
- Reynolds, C. S. 2021, *ARA&A*, 59, 117
- Rodríguez, C. L., Zevin, M., Amaro-Seoane, P., et al. 2019, *PhRvD*, 100, 043027
- Rodríguez, C. L., Zevin, M., Pankow, C., Kalogera, V., & Rasio, F. A. 2016, *ApJL*, 832, L2
- Romero-Shaw, I. M., Talbot, C., Biscoveanu, S., et al. 2020, *MNRAS*, 499, 3295
- Roulet, J., Chia, H. S., Olsen, S., et al. 2021, *PhRvD*, 104, 083010
- Roulet, J., & Zaldarriaga, M. 2019, *MNRAS*, 484, 4216
- Salvesen, G., & Miller, J. M. 2020, *MNRAS*, 500, 3640
- Shao, Y., & Li, X.-D. 2020, *ApJ*, 898, 143
- Shao, Y., & Li, X.-D. 2022, *ApJ*, 930, 26
- Speagle, J. S. 2020, *MNRAS*, 493, 3132
- Stevenson, S. 2022, *ApJL*, 926, L32
- Stevenson, S., Berry, C. P. L., & Mandel, I. 2017, *MNRAS*, 471, 2801
- Talbot, C., Smith, R., Thrane, E., & Poole, G. B. 2019, *PhRvD*, 100, 043030
- Talbot, C., & Thrane, E. 2017, *PhRvD*, 96, 023012
- Talbot, C., & Thrane, E. 2018, *ApJ*, 856, 173
- Taylor, C., & Reynolds, C. S. 2018, *ApJ*, 855, 120
- Thrane, E., & Talbot, C. 2019, *PASA*, 36, e010
- Tichy, W., & Marronetti, P. 2008, *PhRvD*, 78, 081501
- Tiwari, V. 2018, *CQGra*, 35, 145009
- Tong, H., Galadage, S., & Thrane, E. 2022, *PhRvD*, 106, 103019
- Vajpeyi, A., Thrane, E., Smith, R., McKernan, B., & Ford, K. S. 2022, *ApJ*, 931, 82
- Vitale, S., Biscoveanu, S., & Talbot, C. 2022, *A&A*, 668, L2
- Vitale, S., Lynch, R., Sturani, R., & Graff, P. 2017, *CQGra*, 34, 03LT01
- Wysocki, D., Lange, J., & O’Shaughnessy, R. 2019, *PhRvD*, 100, 043012
- Yu, H., Ma, S., Giesler, M., & Chen, Y. 2020, *PhRvD*, 102, 123009
- Zevin, M., & Bavera, S. S. 2022, *ApJ*, 933, 86
- Zevin, M., Bavera, S. S., Berry, C. P. L., et al. 2021, *ApJ*, 910, 152
- Zevin, M., Berry, C. P. L., Coughlin, S., Chatzioannou, K., & Vitale, S. 2020, *ApJL*, 899, L17